



Synthesis-free PET imaging of brown adipose tissue and TSP0 via combination of disulfiram and $^{64}\text{CuCl}_2$

The Harvard community has made this article openly available. [Please share](#) how this access benefits you. Your story matters

Citation	Yang, Jing, Jian Yang, Lu Wang, Anna Moore, Steven H. Liang, and Chongzhao Ran. 2017. "Synthesis-free PET imaging of brown adipose tissue and TSP0 via combination of disulfiram and $^{64}\text{CuCl}_2$." Scientific Reports 7 (1): 8298. doi:10.1038/s41598-017-09018-2. http://dx.doi.org/10.1038/s41598-017-09018-2 .
Published Version	doi:10.1038/s41598-017-09018-2
Citable link	http://nrs.harvard.edu/urn-3:HUL.InstRepos:34375039
Terms of Use	This article was downloaded from Harvard University's DASH repository, and is made available under the terms and conditions applicable to Other Posted Material, as set forth at http://nrs.harvard.edu/urn-3:HUL.InstRepos:dash.current.terms-of-use#LAA

SCIENTIFIC REPORTS

OPEN

Synthesis-free PET imaging of brown adipose tissue and TSPO via combination of disulfiram and $^{64}\text{CuCl}_2$

Jing Yang^{1,2}, Jian Yang^{1,3}, Lu Wang⁴, Anna Moore¹, Steven H. Liang⁴ & Chongzhao Ran¹

PET imaging is a widely applicable but a very expensive technology. On-site synthesis is one important contributor to the high cost. In this report, we demonstrated the feasibility of a synthesis-free method for PET imaging of brown adipose tissue (BAT) and translocator protein 18 kDa (TSPO) via a combination of disulfiram, an FDA approved drug for alcoholism, and $^{64}\text{CuCl}_2$ (termed ^{64}Cu -Dis). In this method, a step-wise injection protocol of $^{64}\text{CuCl}_2$ and disulfiram was used to accomplish the purpose of synthesis-free. Specifically, disulfiram, an inactive ^{64}Cu ligand, was first injected to allow it to metabolize into diethyldithiocarbamate (DDC), a strong ^{64}Cu ligand, which can chelate $^{64}\text{CuCl}_2$ from the following injection to form the actual PET tracer *in situ*. Our blocking studies, western blot, and tissue histological imaging suggested that the observed BAT contrast was due to ^{64}Cu -Dis binding to TSPO, which was further confirmed as a specific biomarker for BAT imaging using [^{18}F]-F-DPA, a TSPO-specific PET tracer. Our studies, for the first time, demonstrated that TSPO could serve as a potential imaging biomarker for BAT. We believe that our strategy could be extended to other targets while significantly reducing the cost of PET imaging.

Positron emission tomography (PET) has been widely used for clinical and preclinical studies, including disease diagnosis, treatment monitoring, and drug development. Compared to other imaging modalities, such as magnetic resonance imaging (MRI), ultrasound, and optical imaging, PET is highly sensitive and quantitative¹. However, the high cost of PET imaging has been the key roadblock for its widespread routine use. The high cost originates from expensive radionuclide production and tracer preparation, which must be conducted on-site¹. Here, we demonstrated the feasibility of a synthesis-free PET imaging method for brown adipose tissue (BAT). With this method, the cost of PET imaging could be dramatically reduced, thus allowing for a widespread application of this technology.

For the purpose of synthesis-free PET imaging, we considered the following criteria: 1) the radionuclide should have a suitable lifetime for delivery and transportation; 2) synthetic components (excluding the radionuclide) should be available in a convenient kit; and 3) the generation of the actual tracers should be very fast or the actual tracers should be formed *in vivo*. To meet the above requirements, we selected ^{64}Cu as the radionuclide due to its reasonable decay lifetime (12.7 hours) and widespread availability. For our proof-of-principle studies we selected BAT as the biological target, because BAT has the following unique features making it a suitable imaging model^{2,3}: 1) BAT in mice is situated away from large organs such as liver, heart, and stomach, and thus signal interference from these large organs is minimal; 2) BAT is a whole mass organ; 3) BAT has a unique triangular physical shape which is easy to distinguish from other tissues.

In the past years, the clinical significance of BAT has been validated through a large-scale analysis of [^{18}F]-FDG PET-CT images and other important studies^{4–8}. BAT is a specialized tissue for thermogenesis in mammals, whose

¹Molecular Imaging Laboratory, Athinoula A. Martinos Center for Biomedical Imaging, Massachusetts General Hospital/Harvard Medical School, Boston, MA, 01890, USA. ²College of Pharmaceutical Sciences, Soochow University, Suzhou, 215006, China. ³School of Pharmacy, China Pharmaceutical University, Nanjing, 210009, China. ⁴Division of Nuclear Medicine and Molecular Imaging & Gordon Center for Medical Imaging, Massachusetts General Hospital/Harvard Medical School, Boston, Massachusetts, 02114, USA. Jing Yang and Jian Yang contributed equally to this work. Correspondence and requests for materials should be addressed to C.R. (email: cran@nmr.mgh.harvard.edu)

function is to dissipate large amounts of chemical/food energy as heat, thus maintaining the energy balance of the whole body^{9–11}. In spite of the fact that investigations of BAT have been ongoing for 70 years, it had been assumed that BAT disappears from the body of adults and has no significant physiological relevance in adult humans^{9,12–14}. This “non-existence” assumption is partially due to the lack of proper imaging methods to “see” the small BAT depots *in vivo*, as only 3%–8% of BAT depots in adults could be clearly visualized with [¹⁸F]-FDG (the most used imaging method) if no cold or drug stimulation is applied^{6,15–17}. However, under stimulated conditions, [¹⁸F]-FDG PET imaging has shown that BAT is still present in 95% of healthy adults in the upper chest, neck, and other locations^{4–6}. This remarkably large difference between non-stimulated and stimulated conditions strongly indicates that [¹⁸F]-FDG PET imaging primarily reflects the activation of BAT, but not BAT mass. Various other imaging methods for BAT are available for preclinical and clinical studies, however most of them are dependent on BAT activation^{18–27}. Therefore, an imaging probe that can consistently report on BAT mass is highly desirable.

In this report, we first conducted a top-down screening, and found that the combination of ⁶⁴CuCl₂ and disulfiram (termed ⁶⁴Cu-Dis) provided high contrast for BAT, which was not affected by BAT activation. We also found that TSPO, a transport protein located on the outer mitochondrial membrane²⁸, was the binding target of ⁶⁴Cu-Dis. We further validated that TSPO is an excellent but unexpected imaging biomarker for BAT using western blot, histology, and PET imaging with TSPO-specific ligand [¹⁸F]-F-DPA.

Results

Screening for BAT-binding ligands. In our previous report³, we have demonstrated that a top-down screening approach could be used for seeking near infrared fluorescence (NIRF) imaging probes for BAT. In that study, we screened 38 NIRF dyes resulting in two hits that we further optimized for high BAT selectivity³. In this report, we used a similar top-down strategy for fast screening of a library of copper ligands, which could be used for fast coordination chemistry with no need for purification. Among the 16 screened ligands, four compounds were considered as positive hits (SI Fig. 1), including disulfiram, diethyldithiocarbamate (DDC, a metabolic product of disulfiram *in vivo*²⁹), cysteamine, and salicylaldehyde.

Using the combination of ⁶⁴CuCl₂ and disulfiram (⁶⁴Cu-Dis) for “synthesis-free” PET imaging.

One of the lead ligands, disulfiram, caught our attention, because it is an FDA approved drug for alcoholism³⁰. Disulfiram, a disulfide compound, does not have a strong affinity to copper. However, when injected *in vivo*, it is reduced to the monomer and releases the thiol group producing diethyldithiocarbamate (DDC), which has a high affinity for copper (II) (Fig. 1a)^{29,31}. Considering that DDC, a metabolic product of disulfiram, is an active copper chelator, we proposed a step-wise injection strategy to realize synthesis-free PET imaging (Fig. 1b). To this end, we injected disulfiram intraperitoneally (40 mg/kg) in mice and allowed 60 minutes for it to metabolize into DDC, the active copper binding form. It has been reported that disulfiram can be rapidly and quantitatively reduced to DDC within 4 minutes and the half-life of DDC in human and dog blood was 70- and 100-minutes³². Considering the above facts, we chose 60-minutes as the interval time between injections of disulfiram and ⁶⁴CuCl₂. Next, we intravenously injected ⁶⁴CuCl₂, which can quickly chelate with DDC *in vivo*. Strikingly, we found that BAT could be easily identified by PET imaging as early as 10 minutes (Fig. 1c), and as late as 48 hours after injections. The uptake of the tracer at 30 minutes after ⁶⁴CuCl₂ injection was 10.6% ID/g (Fig. 1d). More importantly, no apparent signal could be observed from WAT (white adipose tissue), including inguinal and epidermal areas (Fig. 1d and SI Fig. 2a,b), indicating that this method has high BAT selectivity over WAT.

Attaining high BAT/WAT selectivity has been one of the challenges for developing imaging probes for BAT. To confirm the data on BAT/WAT selectivity obtained from *in vivo* PET imaging, we conducted *ex vivo* bio-distribution of BAT and WAT tissues 6 hours after ⁶⁴CuCl₂ injection. We found that interscapular BAT uptake was 13.1% ID/g, which was 10-fold higher than that of interscapular WAT, inguinal WAT, or gonadal WAT (Fig. 1e). Taken together, our *in vivo* imaging data were consistent with the *ex vivo* data, suggesting that ⁶⁴Cu-Dis was highly selective for BAT over WAT. Full *ex vivo* bio-distribution data could be found in SI Fig. 2c.

We also conducted control experiments with ⁶⁴CuCl₂ only, and found that BAT uptake was about 2.47% ID/g (SI Fig. 3a), which was much lower than that with ⁶⁴Cu-Dis (10.6% ID/g), suggesting that disulfiram is necessary for high BAT uptake. Interestingly, we also noticed that the pharmacokinetics of ⁶⁴Cu-Dis and ⁶⁴CuCl₂ only were apparently different (SI Fig. 3b and c). There was no apparent clearance from liver, kidney, and bladder after ⁶⁴CuCl₂ injection within 24 hours, while noticeable clearances from these organs could be observed with ⁶⁴Cu-Dis. Meanwhile, the time courses of BAT uptake with ⁶⁴Cu-Dis and ⁶⁴CuCl₂ only were also evidently different, and clear washing-out could be seen with ⁶⁴Cu-Dis. These differences were likely due to the fact that disulfiram can be rapidly metabolized to its monomer DDC to instantly form Cu(DDC)₂ complex *in vivo*^{29,31}. Taken together, our data suggested that the contribution to BAT uptake from free ⁶⁴CuCl₂ was not significant when our step-wise injection protocol of ⁶⁴Cu-Dis was used for BAT imaging.

***In vivo* BAT imaging with ⁶⁴Cu-Dis.** To investigate whether the “synthesis-free” method can be used to consistently image BAT mass under different conditions, we imaged mice under a normal condition and under cold exposure, which is a standard protocol for BAT activation^{2,33}. For cold exposure, the mice were placed in a cold room at 4 °C for 2 hours before and 1 hour after disulfiram administration. Next, the mice were injected with ⁶⁴CuCl₂ and kept at 4 °C for 30 minutes followed by imaging for 30 minutes (Fig. 2a). BAT uptake was about 10.0% ID/g for normal conditions at 1 hour after ⁶⁴CuCl₂ injection with no significant decrease at 6 hours (SI Fig. 4). Importantly, we found that there was no significant difference in uptake between normal and cold treated groups (Fig. 2b,c). This is contrary to [¹⁸F]-FDG PET and other imaging methods, in which BAT contrast is highly dependent on its activation status. Our data suggested that this synthesis-free method could be used for reporting BAT mass regardless of BAT activation status.

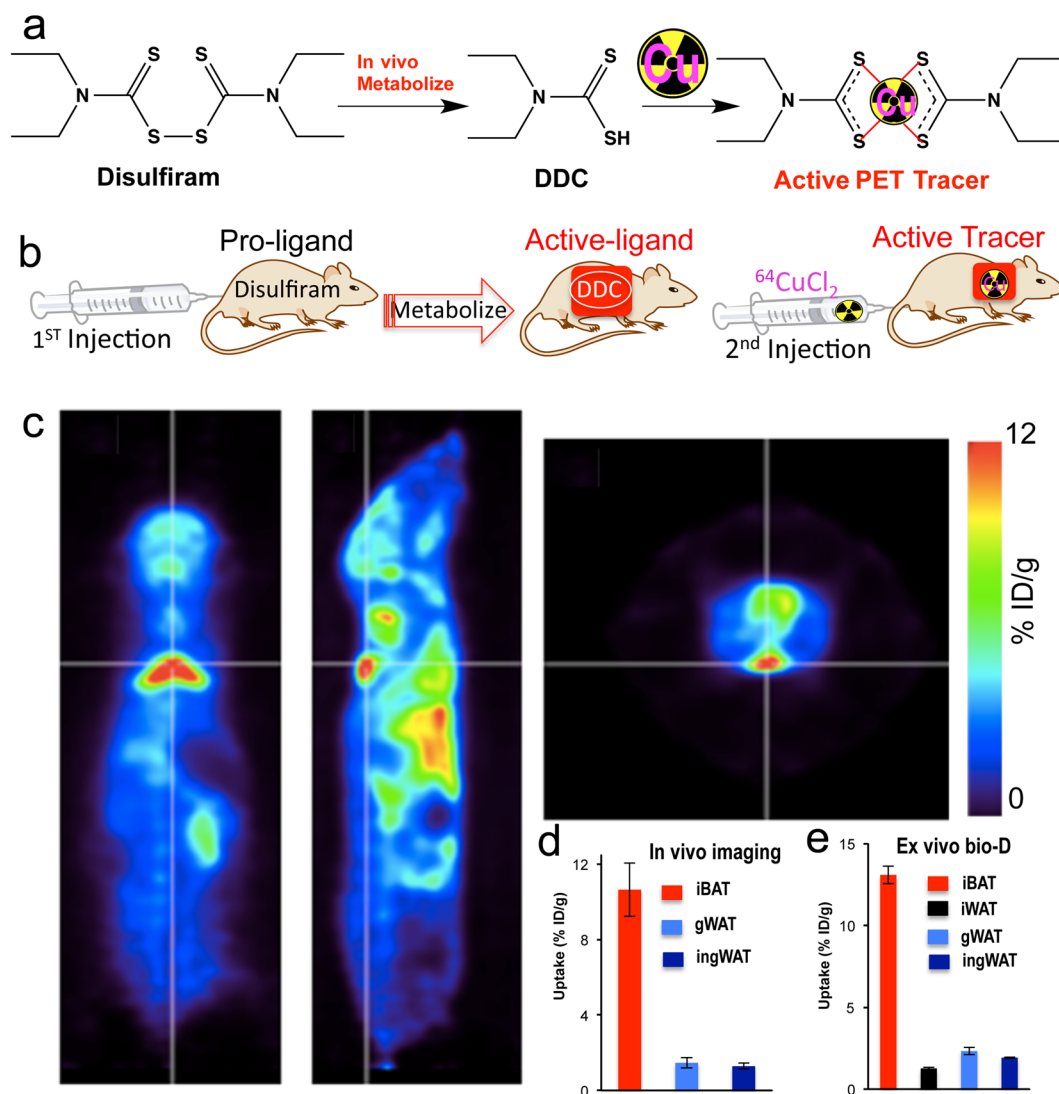


Figure 1. (a) *In-vivo* chemistry of Disulfiram, an inactive copper ligand. It metabolizes to DDC, an active copper ligand, to form the active PET tracer with $^{64}\text{CuCl}_2$ *in vivo*. (b) Diagram of synthesis-free PET imaging via stepwise injection of Disulfiram and $^{64}\text{CuCl}_2$ (^{64}Cu -Dis) 30 minutes after $^{64}\text{CuCl}_2$ injection. (c) Representative PET images of a mouse injected consecutively with Disulfiram and $^{64}\text{CuCl}_2$ (^{64}Cu -Dis) 30 minutes after $^{64}\text{CuCl}_2$ injection. Coronal view (left), sagittal view (right), and transverse view (upper corner). The triangular shape of BAT can be easily identified. (d) Quantitative analysis of the tracer uptake from *in vivo* imaging with ^{64}Cu -Dis in interscapular BAT (iBAT), gonadal WAT (gWAT) and inguinal WAT (ingWAT). (e) *Ex vivo* bio-distribution of the tracer in iBAT, interscapular WAT (iWAT), gWAT and ingWAT.

Blocking studies with TSPO-specific ligand F-DPA. Our *in vivo* and *ex vivo* results revealed that the ^{64}Cu -Dis combination was indeed a synthesis-free method for PET imaging of BAT, however, it was not clear what the molecular binding target was. By surveying the publications reporting on the disulfiram mechanism of action, and found that TSPO could be a target candidate^{34,35}. To investigate whether the uptake of disulfiram or DDC is related to TSPO, we conducted blocking studies using the TSPO specific ligand F-DPA ($K_i = 9 \text{ nM}$) (Compound 3 K in ref. 36, and structure in SI Fig. 5c)³⁶. F-DPA is an analogue of [^{18}F]-DPA-714³⁷, and is a highly selective ligand for TSPO^{36,38}. In these experiments, we intravenously injected 3.0 mg/kg of F-DPA after ip injection of disulfiram, and imaged the mice using the same protocol as above. Images were captured at 1 hour and 6 hours after $^{64}\text{CuCl}_2$ injection. Indeed, we found that F-DPA could effectively block BAT signal at both time points (Fig. 3a,b), with a 35.0% and 60.0% decrease respectively (Fig. 3c,d). Interestingly, we also observed a significant decrease in PET signal from other organs such as heart and kidney (Fig. 3e,f and SI Fig. 5a,b), in which TSPO has reportedly high expression³⁹. Therefore, our data strongly suggested that high BAT contrast was associated with TSPO.

Biological validation of TSPO as a specific biomarker for BAT imaging. To further confirm that TSPO can be used as a specific imaging biomarker for BAT, we performed biological analyses. TSPO, also called

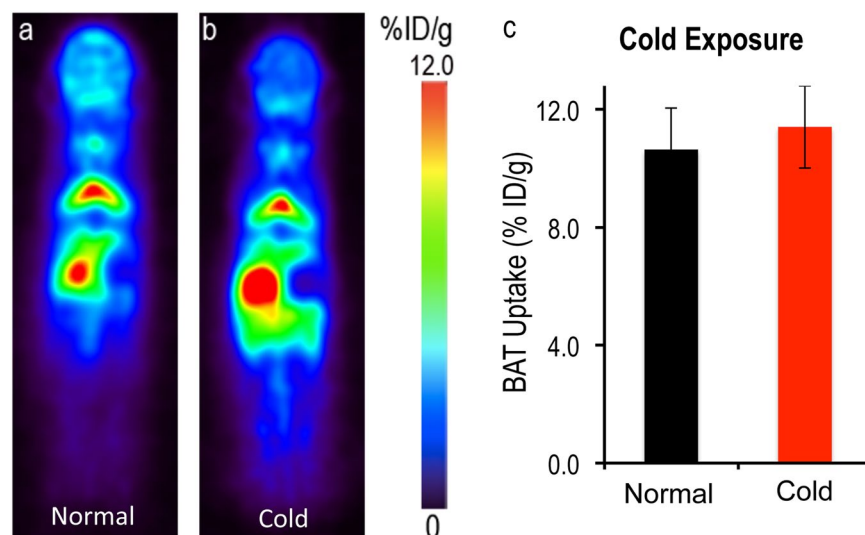


Figure 2. PET images of mice injected ^{64}Cu -Dis under normal and cold exposure conditions. (a) Representative coronal image under a normal condition, (b) Representative coronal image under a cold exposure condition, and (c) Quantitative analysis of (a) and (b). There was no significant difference in uptake between control and cold treated groups ($p=0.359$).

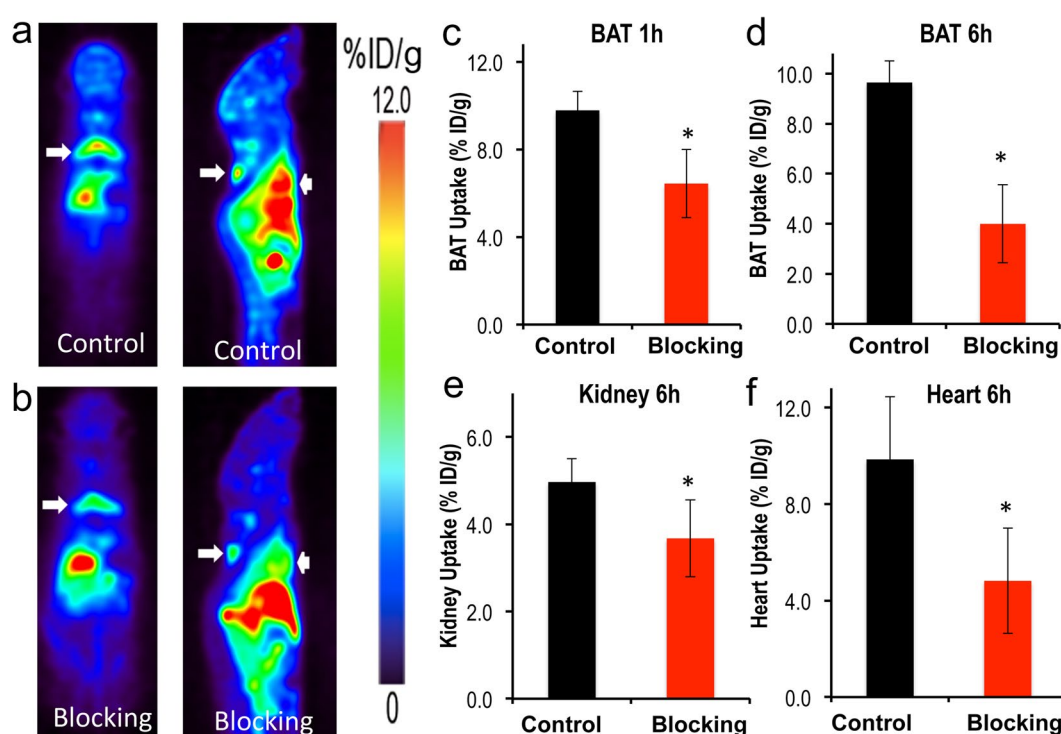


Figure 3. Blocking studies with TSPO ligand F-DPA. (a) Representative PET images of mice injected with ^{64}Cu -Dis without blocking. (b) Representative PET images of mice with ^{64}Cu -Dis with F-DPA blocking. The decreased uptake of ^{64}Cu -Dis can be observed in BAT (white arrow) and heart (arrow head). (c) Quantitative analysis of BAT uptake at 1 hour, (d) Quantitative analysis of BAT uptake at 6 hours, (e) Quantitative analysis of kidney uptake at 6 hours, and (f) quantitative analysis of heart uptake at 6 hours. *Indicates $p < 0.05$.

translocator protein or peripheral benzodiazepine receptor (PBR)^{28, 39}, is located on the outer mitochondrial membrane. It is well known that one of its characteristic features of BAT is its high abundance of mitochondria compared to WAT^{9–11}. It is likely that the abundance of TSPO in BAT is much higher than that in WAT. Nonetheless, no experimental data are available indicating whether TSPO expression in BAT and WAT is significantly different, which is crucial for determining whether TSPO can be used as a specific imaging biomarker for BAT. To answer this question, we compared the qPCR data of TSPO in BAT and WAT, and found that the mRNA

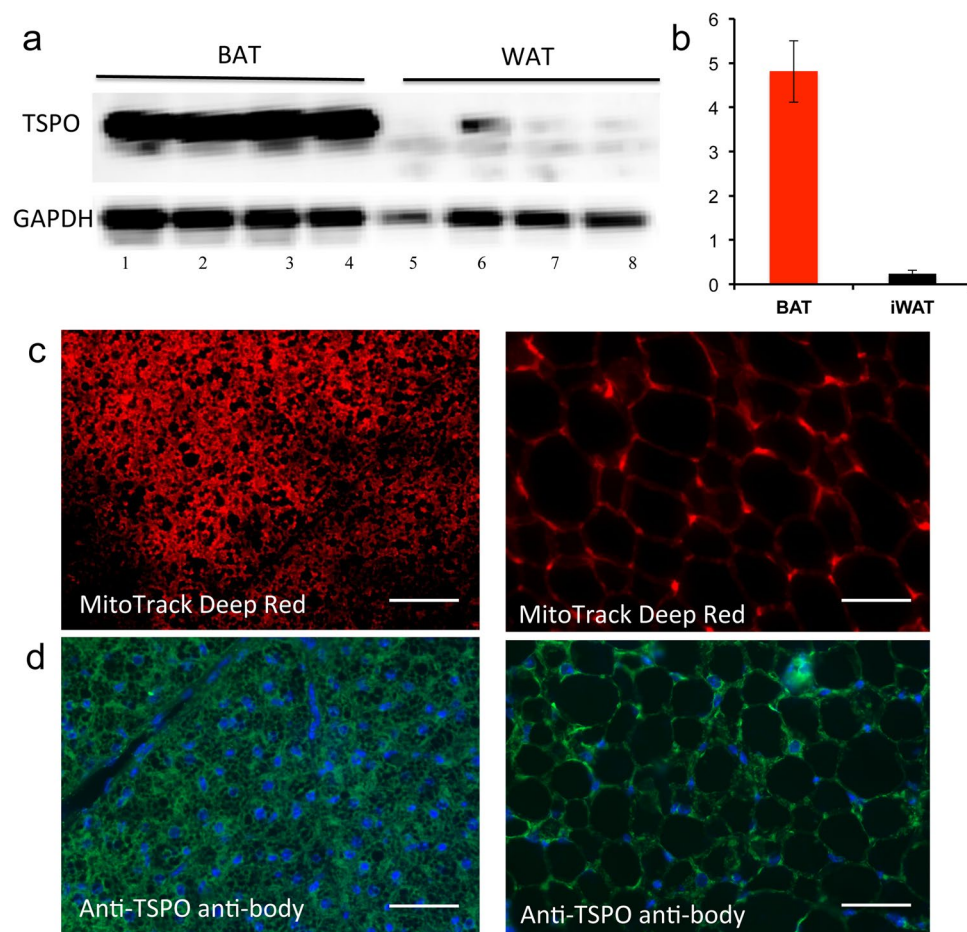


Figure 4. Biological validation of high expression level of TSPO in BAT. (a) Western blot of BAT and WAT tissue extractions with anti-TSPO antibody (lane1–4: four duplicated BAT samples; lane5–8: four duplicated WAT samples), and the full length of blot could be found in SI Fig. 6b, (b) quantification of (a). Note higher TSPO level in BAT compared to WAT. (c) Histological staining of BAT (left) and WAT (right) tissue slices with mitochondria specific dye MitoTrack deep Red, and (d) immunohistological staining of BAT and WAT tissue with anti-TSPO antibody (green) and DAPI for nuclei (blue). Scale bar: 30 μ m.

level in BAT was about 1.5-fold higher than in WAT (SI Fig. 6). To further confirm different levels of TSPO protein expression in BAT and WAT, we performed western blot with anti-TSPO antibody. As shown in Fig. 4a, protein level in BAT was about 20-fold higher than in WAT (Fig. 4a,b, the full length of the blot could be found in SI Fig. 6b). We next investigated the abundance of mitochondria in BAT and WAT tissues using a mitochondria specific dye (MitoTrack deep red FM). As expected, BAT showed much higher fluorescence intensity than WAT (Fig. 4c). In addition, we performed immunological staining of BAT and WAT tissues with anti-TSPO antibody. Figure 4d demonstrated that the abundance of TSPO in BAT was significantly higher than that in WAT. In conclusion, our data for the first time suggested that TSPO could be used as a specific imaging biomarker for BAT.

PET imaging of BAT with TSPO-specific tracer [18 F]-F-DPA. To further validate whether TSPO is a specific imaging biomarker for BAT, we investigated whether existing TSPO-specific PET tracers could provide high contrast for BAT over WAT. To this end, we used [18 F]-labeled TSPO-specific ligand [18 F]-F-DPA^{36–38,40}. We first performed PET imaging in Balb/c mice using a 20-minutes static scan. As seen in Fig. 5a–c, there was a readily identifiable contrast from BAT with a 16% ID/g uptake at 30 minutes after the injection. Moreover, we also compared images at locations with high WAT abundance and found that inguinal and gonadal WAT had minimal uptake (SI Fig. 7).

To further validate the uptake of [18 F]-F-DPA in BAT, we conducted a bio-distribution study in Balb/c mice at 45 minutes after the probe injection. BAT, inguinal WAT and gonadal WAT, brain, liver, and heart were harvested (SI Fig. 8). The bio-distribution data confirmed a higher uptake of the tracer in BAT compared to other organs, suggesting that [18 F]-F-DPA was highly selective for BAT compared to WAT. Taken together, the high uptake in BAT with established TSPO PET ligand supports our hypothesis that TSPO could serve as an imaging biomarker for BAT.

[18 F]-F-DPA uptake is not influenced by BAT activation. To investigate whether [18 F]-F-DPA can be a reliable PET tracer for BAT mass, we conducted PET imaging under BAT activation with cold exposure. Mice

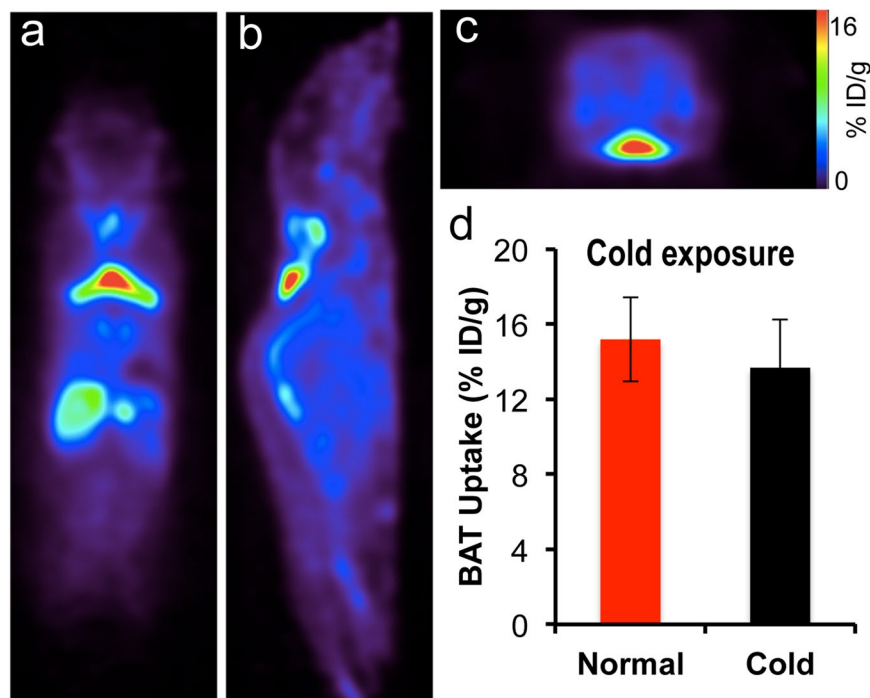


Figure 5. Representative PET images of mice injected with [^{18}F]-F-DPA. (a) Coronal view, (b) sagittal view, and (c) transverse view. The triangular shape of BAT can be clearly identified. (d) Quantitative analysis of BAT uptake under normal and cold exposure. There was no significant difference between these two groups ($p = 0.356$).

were exposed to 4°C for 2 hours before imaging. Our imaging data showed that there were no significant differences between cold treatment and normal condition, indicating that [^{18}F]-F-DPA could serve as a reliable tracer for BAT mass independent of its activation (Fig. 5d). Thompson *et al.* have recently showed that TSPO expression could not be altered by acute cold exposure, which is consistent with the data obtained in our experiment⁴¹. This also suggests that TSPO is a reliable biomarker for BAT mass.

Discussions and Conclusions

PET imaging is immensely useful for both clinical and preclinical applications, however its high cost prevents it from being widely applicable. Requirements for an on-site cyclotron and on-site synthesis are among the major contributors of the high cost. In this report, we demonstrated the feasibility of a synthesis-free PET imaging. Although we demonstrated the application of this method for a specific case that involved imaging of BAT mass, we believe that “pseudo-synthesis-free” and “synthesis-free” methods could be used for other applications as well. “Pseudo-synthesis-free” methods can be realized with fast and strong chelation reaction of ligands with suitable radionuclides. “Synthesis-free” could be feasible if some compounds, which have strong coordination with the radionuclides, could pre-target receptors/enzymes, or if peptides/proteins that have strong chelation with radionuclides could be engineered into specific targets.

In the present study, disulfiram was used as a precursor of a copper ligand, and the actual PET tracer formed *in vivo* via the chelation of $^{64}\text{CuCl}_2$ with DDC, the *in vivo* metabolite of disulfiram. In 2014, Nomura *et al.* reported that disulfiram could serve as an efficient copper delivery drug to the brain in Menkes disease, which is characterized by dysfunction in copper transporting⁴². Brain images from our study (Fig. 1) showed a significant amount of copper accumulated in the brain, which is consistent with the reported results⁴².

Recent large clinical data have clearly demonstrated that BAT is tightly linked to obesity and diabetes^{4–8}. However, imaging methods that can reliably reflect BAT mass are still in shortage. Our data suggested that both ^{64}Cu -Dis and [^{18}F]-F-DPA could be used to reliably report on BAT mass, regardless of the activation status of BAT. This is very different from most used BAT tracers such as [^{18}F]-FDG and others, including MRI and optical imaging probes. Interestingly, compared to [^{18}F]-FDG imaging, the images obtained with our method more reliably contour the unique triangle shape of BAT.

Our studies indicate that the BAT contrast is due to the binding of ^{64}Cu -Dis to TSPO, which is consistent with previous reports^{34,35}. Katz and Gavish reported that disulfiram and DDC were competitive inhibitors for TSPO or PBR (peripheral benzodiazepine receptor)³⁴. They demonstrated that disulfiram and DDC could effectively replace binding of classical TSPO ligands such as Ro5-4864. Gilman *et al.* showed by PET imaging that disulfiram could reduce the uptake of TSPO ligand ^{11}C -Flumazenil in human brain³⁵. In spite of the fact that TSPO has been an imaging target for a long time, particularly for brain imaging, very few reports have emerged utilizing it for peripheral target imaging, and biological evaluation of the high TSPO expression level in BAT is rare⁴¹. In the present study, for the first time, we validated TSPO as an imaging biomarker for BAT.

“Browning”, a process of turning WAT into BAT^{43–45} represents an exciting approach for converting “bad fat” to “good fat” (BAT and beige fat). Since the “browning” process could result in more mitochondria, and our method is capable of detecting the abundance of TSPO in mitochondria, it is reasonable to speculate that our methods have the potential to monitor the browning process, in which the abundance of TSPO increases with the increase of BAT-like cells.

Although TSPO was discovered nearly 40 years ago, its functions in obesity and adipocytes are not well explored. Our studies discovered and confirmed high TSPO expression in BAT, which opened a new avenue for basic BAT research aimed at investigation of biological functions of TSPO. In addition, since TSPO is tightly associated with inflammation²⁸, it is conceivable that ⁶⁴Cu-Dis is also suitable for imaging inflammation in different diseases.

In summary, we demonstrated that a synthesis-free method for PET imaging was feasible, and the combination of ⁶⁴CuCl₂ and disulfiram could be used for BAT imaging. We also validated, for the first time, TSPO as an imaging biomarker for BAT. We believe that our method can be widely applied for TSPO and BAT imaging, and that the synthesis-free strategy could significantly reduce the cost of PET imaging.

Materials and Methods

All of the chemicals were purchased from commercial vendors and used without further purification. Disulfiram was purchased from USP (Cat. No. 1224008, Rockville, MD), and dissolved in a solution of 15% DMSO and 85% Cremophor EL (10 mg/ml). F-DPA and [¹⁸F]-F-DPA were synthesized in Dr. Steven H. Liang laboratory (Massachusetts General Hospital). Balb/c mice and B6C3F1/J mice were purchased from Jackson Laboratory. All animal experiments were approved by the Institutional Animal Use and Care Committee (IACUC) at Massachusetts General Hospital, and carried out in accordance with the approved guidelines.

MicroPET imaging of mice with ⁶⁴Cu-Dis. *In vivo* PET imaging was conducted with 7-month old B6C3F1/J mice. Mice were anesthetized with isoflurane/oxygen for 5 minutes, and then injected intraperitoneally (i.p.) with 100 μ L (40 mg/kg) solution of disulfiram (10 mg/ml). After 60 minutes, mice were injected intravenously (i.v.) with 100 μ L ⁶⁴CuCl₂ (100–150 μ Ci) solution in PBS, pH 7.4. After 0.5- and 6-hours, PET imaging was conducted using a 30-minutes static imaging on a Sophie Biosciences microPET G4 scanner (Culver City, CA, USA). Imaging analysis was conducted using Amide, a Medical Imaging Data Examiner.

Cold exposure treatment. Mice (B6C3F1/J) were placed into cold room (4 °C) for 2 hours, and then i.p. injected with 100 μ L (40 mg/kg) solution of disulfiram (10 mg/ml). The injected mice were then returned to the cold room for 1 hour, and then i.v. injected with 100 μ L ⁶⁴CuCl₂ (100–150 μ Ci) in PBS, pH 7.4. After 30 minutes in the cold room, mice were imaged using a 30-minutes static imaging on the G4 scanner.

Ex vivo bio-distribution of ⁶⁴Cu-Dis. Four-month old Balb/c mice were anesthetized with isoflurane/oxygen for 5 minutes, and then i.p. injected with 100 μ L (40 mg/kg) solution of disulfiram (10 mg/ml). After 60 minutes, mice were i.v. injected with 100 μ L of ⁶⁴CuCl₂ (100–150 μ Ci) solution in PBS, pH 7.4. After six hours, mice were sacrificed, and interscapular BAT, interscapular WAT, inguinal WAT, gonadal WAT and other organs were excised and subjected to counting in a scintillation counter (Packard Cobra II Auto Gamma Scintillation Well Counter).

Blocking studies with TSPO ligand F-DPA. Mice (B6C3F1/J) were i.v. injected with 100 μ L solution (3 mg/kg) of F-DPA in 15% DMSO, 15% Cremophor EL and 70% PBS, and then i.p. injected with 100 μ L (40 mg/kg) solution of disulfiram. The injected mice were returned to the cage for 1 hour, and then i.v. injected with 100 μ L of ⁶⁴CuCl₂ (100–150 μ Ci) in PBS. After 0.5- and 6-hours, mice were imaged using a 30-minute static imaging on the G4 scanner.

Semi-Quantitative PCR Analysis. Total RNA was extracted from the adipose tissue using TRIzol (Invitrogen, Grand Island, NY). The cDNA was synthesized by iScriptTM system (Bio-Rad, Hercules, CA). Reverse transcription reaction was performed using a PTC-100 programmable thermal controller (MJ Research Inc., Waltham, MA). A real time PCR was performed using an iTaqTM universal STBR[®] green Supermix (Bio-Rad, Hercules, CA) in an Mx3005 P qPCR thermocycler (Agilent Technologies, Santa Clara, CA). All values were normalized to cyclophilin expression and further analyzed using the $\Delta\Delta C_T$ method. The sequences of primers used in the semi-quantitative PCR were as following: TSPO (forward: 5'-CCATGGGGTATGGCTCCTACA-3', reverse: 5'-CCAAGGGAACCATAGCGTCC-3'); cyclophilin (forward: 5'-GGAGATGGCAGGAGGAA-3', reverse: 5'-GCCCCGTAGTGCTTCAGCTT-3').

Western blotting with anti-TSPO antibody. Adipose tissue was homogenized in a RIPA lysis buffer (Millipore) supplemented with protease and phosphatase inhibitor cocktails (Thermo Scientific). Homogenates were centrifuged at 13,000 r.p.m. at 4 °C for 20 minutes, and the supernatants were used as tissue lysates. Protein concentration was determined by BCA protein assay. Seventy micrograms of protein lysate was separated in a 4–20% SDS-PAGE gel. The separated proteins were transferred to a polyvinylidene difluoride (PVDF) membrane, which was then blocked in 5% NFDM at room temperature for 2 hours. After blocking, the membrane was incubated with anti-TSPO primary antibody in TBST buffer (1:1000 dilution, Cell Signaling) at 4 °C overnight. After washing with TBST buffer, the membrane was incubated with the secondary antibody (goat anti-rabbit IgG (H + L), Invitrogen) for 1 hour at room temperature. Western Pico Chemiluminescent Substrate (Thermo scientific) was used to visualize the bands. The images were acquired with IVIS[®]Spectrum (Perkin Elmer, Hopkinton MA) using bioluminescence imaging setting. PageRuler Plus Prestained Protein Ladder (Thermo Fisher) (10–250 KD) was used as a molecular weight marker.

Immunohistochemistry with anti-TSPO antibody and histochemical staining with MitoTracker. Adipose tissue was fixed in 4% formaldehyde at room temperature for 24 hours, embedded in paraffin and cut into 5-micron slices. For immunostaining, heat mediated antigen retrieval was first performed using Antigen Retrieval Citra Plus Solution (Biogenex), and then the sections were blocked with 5% NFDM for 1 hour at room temperature. After that, the samples were incubated with anti-PBR/TSPO antibody (Abcam, ab109497) diluted in a blocking buffer overnight at 4 °C. After washing with TBST, the samples were incubated with secondary FITC-labeled antibody for 1 hour at room temperature and counterstained with DAPI. For Mitochondria staining, deparaffinized sections were incubated with MitoTracker probes (500 nM) (Invitrogen, MitoTracker® Deep Red FM, cat. No. M22426) for 30 minutes at room temperature. Images were captured using a Nikon ECLIPSE 50i fluorescence microscope.

In vivo PET imaging with [¹⁸F]-F-DPA. *In vivo* PET imaging was conducted with C57BL/6J mice. For cold treatment, mice were placed in the cooled room (4 °C) for 2 hours. Mice were i.v. injected with 100 μL of 20–30 μCi [¹⁸F]-F-DPA in 10% ethanol saline. PET imaging was conducted using a 20-minutes static scan on a Sofie Biosciences microPET G4 scanner under short anesthesia (isoflurane/O₂) (2–3 minutes). Imaging analysis was conducted with Amide.

References

- Massoud, T. F. & Gambhir, S. S. Molecular imaging in living subjects: seeing fundamental biological processes in a new light. *Genes Dev* **17**, 545–580 (2003).
- Zhang, X., Kuo, C., Moore, A. & Ran, C. *In Vivo* Optical Imaging of Interscapular Brown Adipose Tissue with 18F-FDG via Cerenkov Luminescence Imaging. *PLoS One* **8**, e62007 (2013).
- Zhang, X. *et al.* Curcumin analogues as selective fluorescence imaging probes for brown adipose tissue and monitoring browning. *Sci. Rep.* **5**, 13116 (2015).
- Cypess, A. M. *et al.* Identification and importance of brown adipose tissue in adult humans. *The New England journal of medicine* **360**, 1509–1517 (2009).
- Virtanen, K. A. *et al.* Functional brown adipose tissue in healthy adults. *The New England journal of medicine* **360**, 1518–1525 (2009).
- van Marken Lichtenbelt, W. D. *et al.* Cold-activated brown adipose tissue in healthy men. *N. Engl. J. Med.* **360**, 1500–1508 (2009).
- Nedergaard, J., Bengtsson, T. & Cannon, B. Unexpected evidence for active brown adipose tissue in adult humans. *American journal of physiology. Endocrinology and metabolism* **293**, E444–452 (2007).
- Tran, T. T. & Kahn, C. R. Transplantation of adipose tissue and stem cells: role in metabolism and disease. *Nature reviews. Endocrinology* **6**, 195–213 (2010).
- Cannon, B. & Nedergaard, J. Brown adipose tissue: function and physiological significance. *Physiol. Rev.* **84**, 277–359 (2004).
- Richard, D. & Picard, F. Brown fat biology and thermogenesis. *Frontiers in bioscience: a journal and virtual library* **16**, 1233–1260 (2011).
- Ouellet, V. *et al.* Brown adipose tissue oxidative metabolism contributes to energy expenditure during acute cold exposure in humans. *The Journal of clinical investigation* **122**, 545–552 (2012).
- Lowell, B. B. & Flier, J. S. Brown adipose tissue, beta 3-adrenergic receptors, and obesity. *Annu. Rev. Med.* **48**, 307–316 (1997).
- Stephens, M., Ludgate, M. & Rees, D. A. Brown fat and obesity: the next big thing? *Clin. Endocrinol. (Oxf.)* **74**, 661–670 (2011).
- Koppen, A. & Kalkhoven, E. Brown vs white adipocytes: the PPARgamma coregulator story. *FEBS Lett.* **584**, 3250–3259 (2010).
- Cohade, C., Mourtzikos, K. A. & Wahl, R. L. “USA-Fat”: prevalence is related to ambient outdoor temperature-evaluation with 18F-FDG PET/CT. *Journal of nuclear medicine: official publication, Society of Nuclear Medicine* **44**, 1267–1270 (2003).
- Lee, P., Ho, K. K. & Fulham, M. J. The importance of brown adipose tissue. *The New England journal of medicine* **361**, 418, author reply 419–420 (2009).
- Lidell, M. E. & Enerback, S. Brown adipose tissue—a new role in humans? *Nature reviews. Endocrinology* **6**, 319–325 (2010).
- Hu, H. H., Smith, D. L. Jr., Nayak, K. S., Goran, M. I. & Nagy, T. R. Identification of brown adipose tissue in mice with fat-water IDEAL-MRI. *Journal of magnetic resonance imaging: JMIR* **31**, 1195–1202 (2010).
- Madar, I., Isoda, T., Finley, P., Angle, J. & Wahl, R. 18F-fluorobenzyl triphenyl phosphonium: a noninvasive sensor of brown adipose tissue thermogenesis. *Journal of nuclear medicine: official publication, Society of Nuclear Medicine* **52**, 808–814 (2011).
- Peng, X. G. *et al.* Comparison of brown and white adipose tissue fat fractions in ob, seipin, and Fsp27 gene knockout mice by chemical shift-selective imaging and (1)H-MR spectroscopy. *American journal of physiology. Endocrinology and metabolism* **304**, E160–167 (2013).
- Bartelt, A. *et al.* Brown adipose tissue activity controls triglyceride clearance. *Nat. Med.* **17**, 200–205 (2011).
- Branca, R. T. *et al.* Detection of brown adipose tissue and thermogenic activity in mice by hyperpolarized xenon MRI. *Proc. Natl. Acad. Sci. USA* **111**, 18001–18006 (2014).
- Nakayama, A., Bianco, A. C., Zhang, C. Y., Lowell, B. B. & Frangioni, J. V. Quantitation of brown adipose tissue perfusion in transgenic mice using near-infrared fluorescence imaging. *Mol. Imaging* **2**, 37–49 (2003).
- Azhdarinia, A. *et al.* A peptide probe for targeted brown adipose tissue imaging. *Nature communications* **4**, 2472 (2013).
- Rice, D. R., White, A. G., Leevy, W. M. & Smith, B. D. Fluorescence Imaging of Interscapular Brown Adipose Tissue in Living Mice. *Journal of materials chemistry. B, Materials for biology and medicine* **3**, 1979–1989 (2015).
- Chen, Y. I. *et al.* Anatomical and Functional Assessment of Brown Adipose Tissue by Magnetic Resonance Imaging. *Obesity* **20**, 1519–1526 (2012).
- Khanna, A. & Branca, R. T. Detecting brown adipose tissue activity with BOLD MRI in mice. *Magnetic resonance in medicine: official journal of the Society of Magnetic Resonance in Medicine/Society of Magnetic Resonance in Medicine* **68**, 1285–1290 (2012).
- Li, F., Liu, J., Garavito, R. M. & Ferguson-Miller, S. Evolving understanding of translocator protein 18 kDa (TSPO). *Pharmacol. Res.* **99**, 404–409 (2015).
- Johansson, B. & Stankiewicz, Z. Bis-(diethyldithiocarbamate) copper complex: a new metabolite of disulfiram? *Biochem. Pharmacol.* **34**, 2989–2991 (1985).
- Wright, C. & Moore, R. D. Disulfiram treatment of alcoholism. *The American journal of medicine* **88**, 647–655 (1990).
- Szerdahelyi, P. & Kasa, P. Regional differences in the uptake of exogenous copper into rat brain after acute treatment with sodium diethyldithiocarbamate. A histochemical and atomic absorption spectrophotometric study. *Histochemistry* **86**, 627–632 (1987).
- Cobby, J., Mayersohn, M. & Selliah, S. The rapid reduction of disulfiram in blood and plasma. *The Journal of pharmacology and experimental therapeutics* **202**, 724–731 (1977).
- Wu, C. *et al.* Brown adipose tissue can be activated or inhibited within an hour before 18F-FDG injection: a preliminary study with microPET. *Journal of biomedicine & biotechnology* **2011**, 159834 (2011).
- Katz, Y., Weizman, R., Weizman, A. & Gavish, M. Disulfiram and diethyldithiocarbamate are competitive inhibitors at the peripheral benzodiazepine receptor. *The Journal of pharmacology and experimental therapeutics* **262**, 394–397 (1992).

35. Gilman, S. *et al.* Effects of disulfiram on positron emission tomography and neuropsychological studies in severe chronic alcoholism. *Alcohol. Clin. Exp. Res.* **20**, 1456–1461 (1996).
36. Salleri, S. *et al.* 2-Arylpirazolo[1,5-a]pyrimidin-3-yl acetamides. *New potent and selective peripheral benzodiazepine receptor ligands.* *Biorg. Med. Chem.* **9**, 2661–2671 (2001).
37. Doorduyn, J. *et al.* [11C]-DPA-713 and [18F]-DPA-714 as new PET tracers for TSPO: a comparison with [11C]-(R)-PK11195 in a rat model of herpes encephalitis. *Molecular imaging and biology: MIB: the official publication of the Academy of Molecular Imaging* **11**, 386–398 (2009).
38. Reynolds, A. *et al.* Pyrazolo[1,5-a]pyrimidine acetamides: 4-Phenyl alkyl ether derivatives as potent ligands for the 18 kDa translocator protein (TSPO). *Biorg. Med. Chem. Lett.* **20**, 5799–5802 (2010).
39. Woods, M. J. & Williams, D. C. Multiple forms and locations for the peripheral-type benzodiazepine receptor. *Biochem. Pharmacol.* **52**, 1805–1814 (1996).
40. Wang, L. *et al.* A Facile Radiolabeling of [18F]FDPA via Spirocyclic Iodonium Ylides: Preliminary PET Imaging Studies in Preclinical Models of Neuroinflammation. *J. Med. Chem.* **60**, 5222–5227 (2017).
41. Thompson, M. M., Manning, H. C. & Ellacott, K. L. Translocator protein 18 kDa (TSPO) is regulated in white and brown adipose tissue by obesity. *PLoS One* **8**, e79980 (2013).
42. Nomura, S. *et al.* PET imaging analysis with ⁶⁴Cu in disulfiram treatment for aberrant copper biodistribution in Menkes disease mouse model. *Journal of nuclear medicine: official publication, Society of Nuclear Medicine* **55**, 845–851 (2014).
43. Kajimura, S. *et al.* Regulation of the brown and white fat gene programs through a PRDM16/CtBP transcriptional complex. *Genes Dev.* **22**, 1397–1409 (2008).
44. Farmer, S. R. Molecular determinants of brown adipocyte formation and function. *Genes Dev.* **22**, 1269–1275 (2008).
45. Wilson-Fritch, L. *et al.* Mitochondrial remodeling in adipose tissue associated with obesity and treatment with rosiglitazone. *The Journal of clinical investigation* **114**, 1281–1289 (2004).

Acknowledgements

This work was supported by NIH/NIDDK R56DK108813 award (C.R.). The authors would also like to thank Pamela Pantazopoulos, B.S. for proofreading this manuscript. We also thank China Scholarship Council of Ministry of Education of China for supporting (J.Y. and J.Y.).

Author Contributions

J.Y., J.Y. and C.R. designed the study; J.Y., J.Y., L.W. and C.R. performed experiments; J.Y. and C.R. wrote the manuscript; S.L. and A.M. provided suggestions for the experiments and critical comments on the manuscript; C.R. supervised the study.

Additional Information

Supplementary information accompanies this paper at doi:[10.1038/s41598-017-09018-2](https://doi.org/10.1038/s41598-017-09018-2)

Competing Interests: The authors declare that they have no competing interests.

Publisher's note: Springer Nature remains neutral with regard to jurisdictional claims in published maps and institutional affiliations.



Open Access This article is licensed under a Creative Commons Attribution 4.0 International License, which permits use, sharing, adaptation, distribution and reproduction in any medium or format, as long as you give appropriate credit to the original author(s) and the source, provide a link to the Creative Commons license, and indicate if changes were made. The images or other third party material in this article are included in the article's Creative Commons license, unless indicated otherwise in a credit line to the material. If material is not included in the article's Creative Commons license and your intended use is not permitted by statutory regulation or exceeds the permitted use, you will need to obtain permission directly from the copyright holder. To view a copy of this license, visit <http://creativecommons.org/licenses/by/4.0/>.

© The Author(s) 2017